Effect of nickel addition on the microstructure and corrosion resistance properties of porous alumina composites shaped with sugarcane bagasse pore-forming agent

Effect of nickel addition on the microstructure and corrosion resistance properties of porous alumina composites shaped with sugarcane bagasse pore-forming agent

T T Dele-Afolabi[1*], M A Azmah Hanim[1], M Norkhairunnisa[2], S Sobri[3], R Calin[4] and O J Ojo-Kupoluyi[1]

[1] Department of Mechanical and Manufacturing Engineering, Faculty of Engineering, Universiti Putra Malaysia, 43400 UPM Serdang Selangor, Malaysia.
[2] Department of Aerospace Engineering, Faculty of Engineering, Universiti Putra Malaysia, 43400 UPM Serdang Selangor, Malaysia.
[3] Department of Chemical and Environmental Engineering, Faculty of Engineering, Universiti Putra Malaysia, 43400 UPM Serdang Selangor, Malaysia.
[4] Department of Metallurgy and Materials Science Engineering, Faculty of Engineering, Kirikkale University, Turkey.

[*]Corresponding author: deleafolabitemitope@gmail.com

Abstract. In this study, the effect of nickel (Ni) addition on the microstructure and corrosion resistance properties of porous alumina (Al_2O_3) composites shaped with sugarcane bagasse pore-forming agent were evaluated. Plain and Ni-reinforced porous alumina sampels (Al_2O_3-xNi-RH; x = 2, 4, 6 and 8wt%) were prepared using the powder metallurgy method. Experimental results showed that the porosity (50.4-57.1vol%) and the pore size (62-109μm) of the porous alumina composites increased with rising content of Ni reinforcement. The XRD results showed that the Al_2O_3 matrix and Ni reinforcement reacted during the heat treatment process to produce nickel aluminate ($NiAl_2O_4$) spinel. Corrosion resistance results showed that the porous alumina composites exhibited better chemical stability in strong alkali solution as compared with strong acid solution.

1. Introduction

Highly porous ceramic materials can be used in diverse technological applications such as combustion burners, thermal insulation, molten metal filtration, wastewater treatment among others [1-4]. In recent times, alumina has been employed as the preffered ceramic material for developing porous materials. However, the intrinsic brittleness and the harsh operating conditions especially in highly corrosive mediums limit their usage as separation membrane units [5-7]. Hence, it is important for researchers to employ the composite approach in revamping the plain porous alumina ceramic so as to enhance the chemical stability needed for operation under aggressive working ambience.

Thus far, nickel (Ni), an outstanding metal material has aroused the interest of researchers to upgrade the intrinsic properties of ceramics due to its excellent corrosion resistance and relatively high melting temperature among others [8-11]. Even though the investigations were based on fully dense Al_2O_3/Ni composites fabricated either through preform infiltration or hot isostatic pressing, the synergy between the properties between the alumina matrix and nickel particulate resulted in the enhancement of the

corrosion resistance properties and microstructural refinement of the composites as compared with the monolithic counterpart.

Meanwhile, most of the existing investigations have reported the development of porous ceramic composites by employing the multi-phasic ceramics approach [12,13], fiber reinforcement [14,15] and polymer reinforcement[16]. Besides the difficulties including matrix warpage and pore occlusion associated with the usage of these fabrication methods for developing porous ceramic composites, additional setbacks arise from the dispersion of the nickel particles and pore size limitation which therefore affect the implementation of the composite approach in enhancing the traditional porous alumina ceramics [17,18].

With a view to developing high performance porous alumina composites for functional application, porous Al_2O_3/Ni composites were developed using the pore-forming agent method in the current study. So far, pore-forming agents from agricultural waste materials have exhibited excellent results in the development of porous ceramic materials. Hence, in order to gain deeper insight into the joint effect of the composite approach and the fabrication technique, different formulations of Ni-reinforced porous alumina composites were shaped with sugarcane bagasse pore former followed by a systematic evaluation of the microstructure and corrosion resistance properties.

2. Experimental Procedure

Pure alumina powder (Al_2O_3), nickel (Ni) particles and sugarcane bagasse (SCB) powder were used as the matrix, reinforcement and pore-forming agent respectively to develop porous Al_2O_3/Ni ceramic composites with sample formulations of Al_2O_3-10SCB, Al_2O_3-2Ni-10SCB, Al_2O_3-4Ni-10SCB, Al_2O_3-6Ni-10SCB and Al_2O_3-8Ni-10SCB. Firstly, alumina and nickel particles were wet milled in ethanol for 12 h at 550 rpm using a planetary mono mill (Fritsch Pulverisette 7). Thereafter, the composite slurry was dried and later milled for 6 h to break the lumps from the dried slurry. Acid treated sugarcane bagasse was introduced as the pore-forming agent to the composite blend through dry milling process for 1 h at 300 rpm and later subjected to manual mixing process for 5mins to homogenize the binding agent (10 wt% sucrose solution) with the powder blends.

Afterwards, all the sample formulations were compacted at 95 MPa and the green pellets were subjected to two different heat-treatment processes. Firstly, samples were subjected to an organic burnout process where the heating and cooling rates were fixed at 1 °C/min for a stepwise temperature increment and 1 h dwell time at each of 200, 300, 500, and 800 °C. Secondly, the samples were sintered at 1450 °C using 5 °C/min as the heating rate. The flowchart for the development of the porous Al_2O_3/Ni ceramic composites is presented in Figure 1.

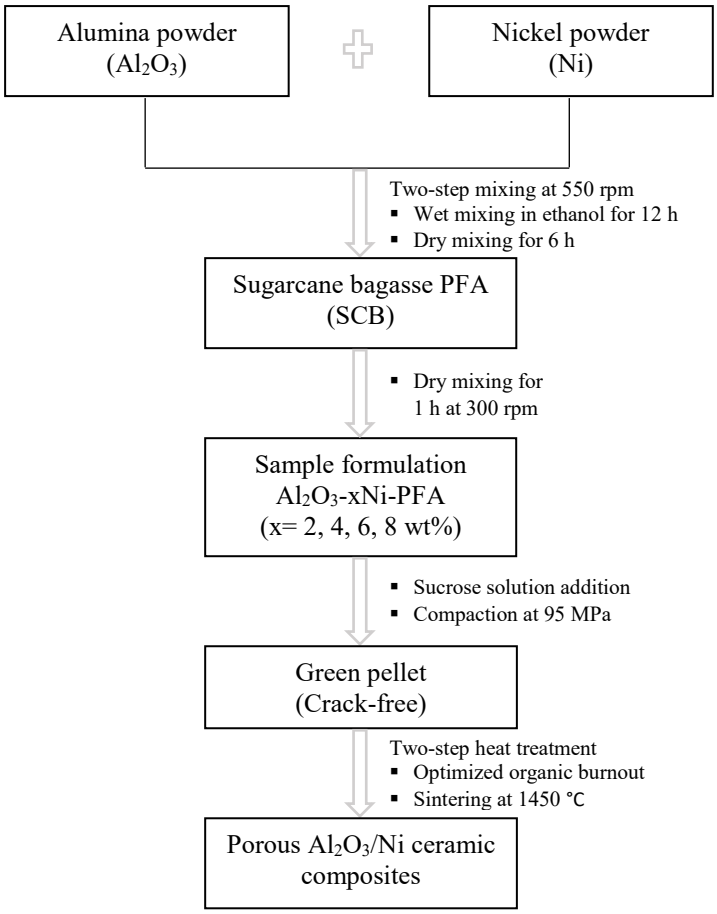

Figure 1. Flowchart for the development of porous Al_2O_3/Ni ceramic composites.

The density and porosity values of the porous Al_2O_3/Ni ceramic composites were measured by employing the Archimedes' principle. In order to measure the total porosity, the theoretical densities of fully dense composites (Alumina= 3.96 g/cm^3; Nickel= 8.91 g/cm^3) were determined using the rule of mixtures. The linear shrinkage was measured by using a Vernier Caliper. The microstructure of the samples was observed using the Field Emission Scanning Electron Microscope (FESEM; FEI, Nova Nanosem 230) and the pore size was subsequently measured by using the ImageJ software. Phase composition of the samples was analysed by using the X-ray diffractometer (Philips X'PERT PRO PANALYTICAL) with CuKα radiation (wavelength = 1.5406 Å) at 40 kV and 40 mA. For the corrosion resistance investigation, the porous composite samples with dimension of 18.5 mm x 4.5 mm (diameter x thickness) were ultrasonically cleaned in ethanol, dried and weighed. Thereafter, the samples were placed into 10 wt% NaOH and 20 wt% H_2SO_4 hot aqueous solutions (according to the Chinese standard, GB/T 1970-96) and after the corrosion process, samples were rinsed in deionised water to remove the corrosion residue. The mass loss after corrosion at 110°C for 2 h - 8 h was measured and the microstructures of the corroded samples were analysed using the FESEM images.

3. Results and Discussion

3.1. Phase analysis

Figure 2 presents the XRD result of the plain and the composite porous samples having 4 wt% Ni reinforcement. It can be observed from the plot that corundum (Al_2O_3) in the plain sample has been replaced by a new phase of nickel aluminate ($NiAl_2O_4$) spinel. Equation 1 presents the reaction for the formation of the $NiAl_2O_4$ spinel. It is noteworthy that no Al_2O_3 or Ni was detected in the porous composite samples which implies the complete reaction of the starting nickel reinforcement with the alumina matrix to form spinel during the heat treatment phase under high-pressure oxygen actuated by the existence of a highly porous microstructure in the green compacts. Moreover, it is important to mention that the formation of the ferrierite peak in the porous composite sample was as a result of the trapped H_2O gas and the strong affinity of hydrated Ni^+ to tectosilicate (ferrierite) group. A similar finding was reported by Dalconi et al. [19].

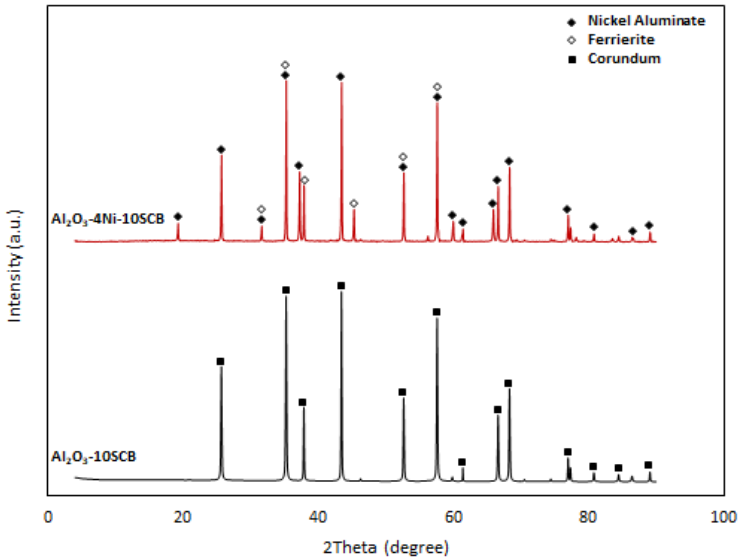

Figure 2. XRD patterns of plain and composite porous ceramics sintered at 1450 °C.

$$Ni + Al_2O_3 + \frac{1}{2}O_2 \leftrightarrow NiAl_2O_4 \qquad (1)$$

3.2. Porosity and microstructure

Figure 3 shows the variations of density and porosity of composite porous alumina samples as a function of different weight fractions of Ni reinforcement. It can be observed that while the density of the porous ceramic composites decreased with increasing Ni reinforcement, total porosity values exhibited a corresponding increase. This finding can be ascribed to the existence of thermal expansion mismatch and poor wettability between the liquid Ni and Al_2O_3 matrix during the heat treatment process. A similar finding was reported elsewhere, where the high magnetic and electrostatic interractions of Ni particles actuated the defective densification process in Ni-reinforced alumina composites [20].

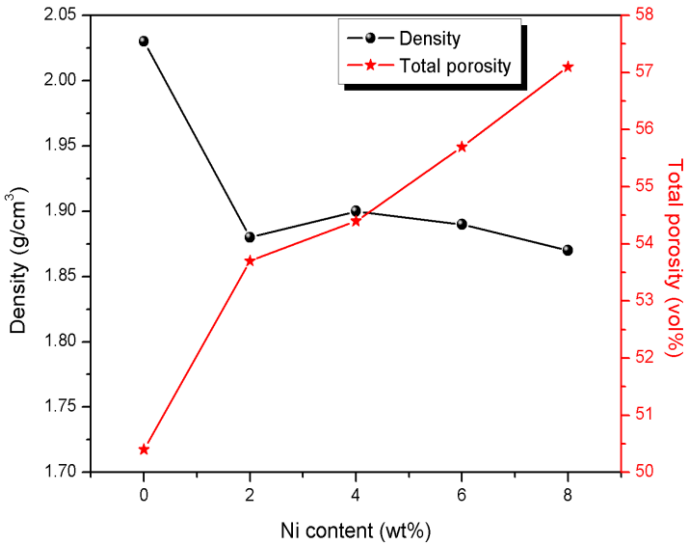

Figure 3. Variations of density and porosity of composite porous alumina samples as a function of different weight fractions of Ni reinforcement.

Figure 4 presents the microstructures of the plain and Ni-reinforced porous ceramic composites with varying contents of Ni reinforcement as well as the EDS spectrum of the composite samples. More so, Table 1 summarizes the pore sizes of the plain and composite samples. It can be evidenced that the pore cavities increased with rising Ni content due to defective densification and poorly crystallized nickel aluminate spinel. Meanwhile, it can be seen that samples having 2 and 4 wt% Ni reinforcement exhibited lesser pore sizes relative to the plain sample. The pore contraction in these samples can best be explained by the report of Hashimoto et al. where volume expansion within the range of 5-7 % was recorded during the formation of the spinel phase in porous $MgAl_2O_4$ spinel produced from alumina and magnesium oxide particles [21].

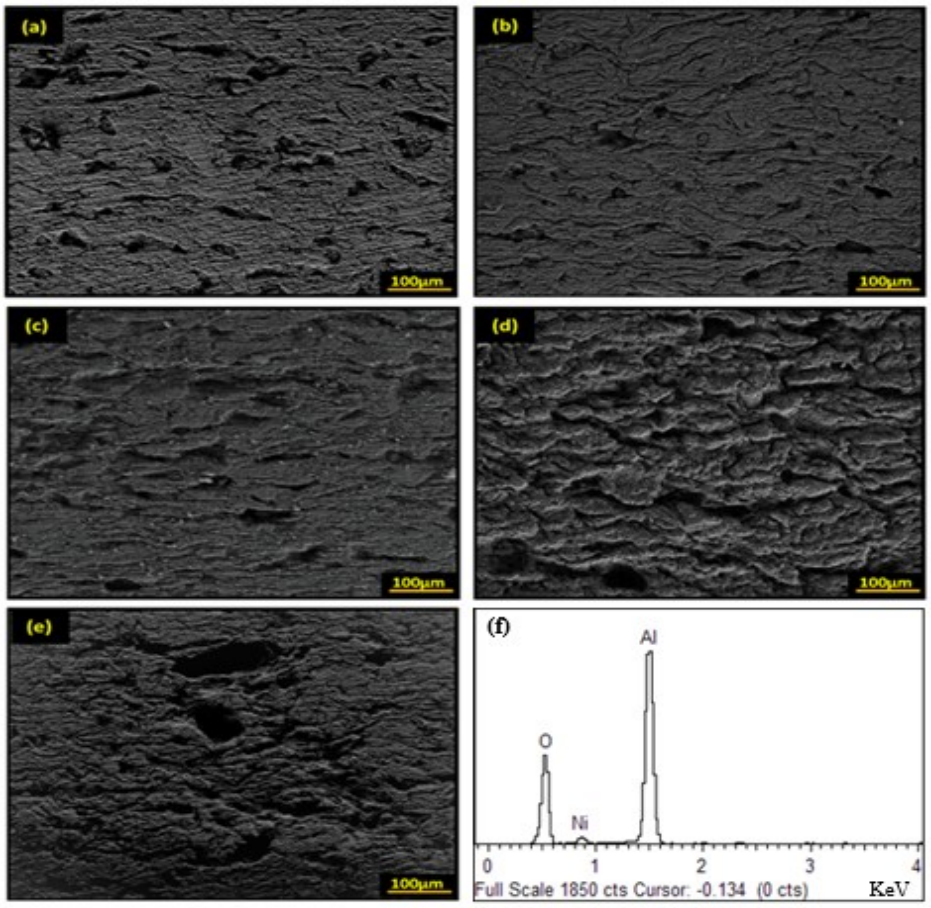

Figure 4. FESEM micrographs showing the pore morphology of samples reinforced with (a) 0 wt% Ni (b) 2 wt% Ni (c) 4 wt% Ni(d) 6 wt% Ni(e) 8 wt% Ni and (f) EDS spectrum for the composite samples.

Table 1. Summary of plain and composite porous alumina sample formulations and their corresponding density, porosity, pore size distribution (median values are boldface).

Sample formulation	Density (g/cm^3)	Total Porosity (vol%)	Pore size Distribution (µm)		
			D_{10}	D_{50}	D_{90}
Al_2O_3-10SCB	2.03	50.4	51	84	127
Al_2O_3-2Ni-10SCB	1.88	53.7	33	62	96
Al_2O_3-4Ni-10SCB	1.90	54.4	42	78	118
Al_2O_3-6Ni-10SCB	1.89	55.7	46	92	139
Al_2O_3-8Ni-10SCB	1.87	57.1	52	109	164

3.3. Corrosion resistance test

Figure 5 presents the percentage mass loss as a function of corroding time for the plain and Ni-reinforced porous alumina ceramic composites. As observed, both the plain and composite samples showed superior resistance to corrosion in the 10 wt% NaOH than the 20 wt% H_2SO_4. Regardless of the sample formulation, it can be evidenced that the mass loss values in acidic and alkaline solutions increased with increasing corroding time. Meanwhile, the unabated evolution of poorly crystallized $NiAl_2O_4$ spinel with increasing Ni reinforcement mainly accounts for the abysmal performance of the composite samples in the corrosive mediums relative to the plain counterpart. A similar finding was reported by Allende-Mata et al. where it was observed that the $NiAl_2O_4$ spinel was unstable in different corrosive mediums owing to the dissolution and reaction between the $NiAl_2O_4$ spinel and the corrosive mediums to form other spinel or metal oxides [22]. Also notable from the figure is the fact that the Al_2O_3-4Ni-10SCB composite sample exhibited a superior corrosion resistance overtime than other composite samples which was due to the relatively high density registered for this particular sample.

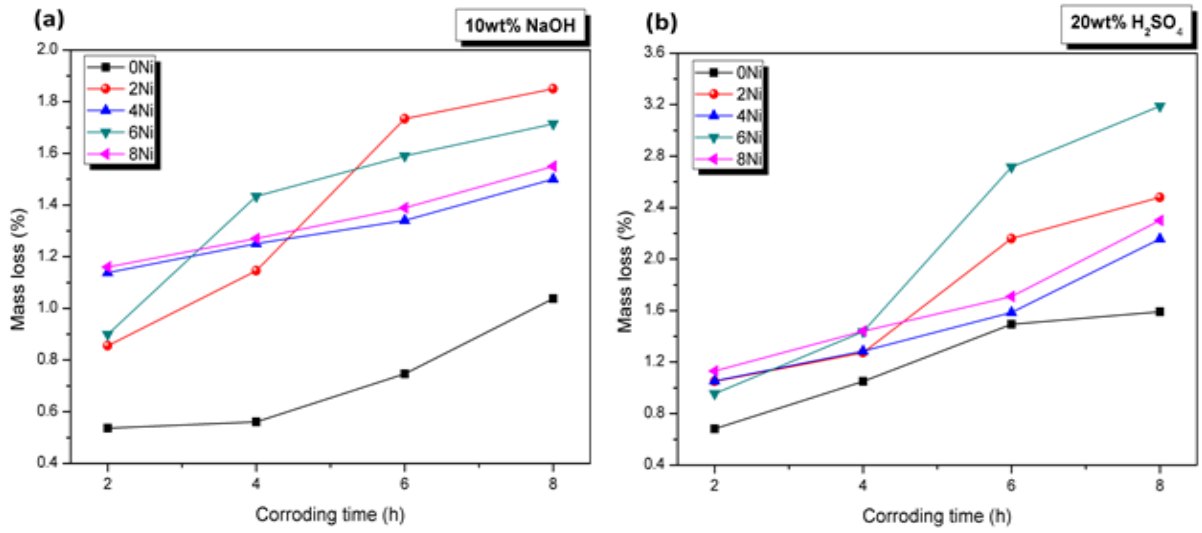

Figure 5. Mass loss of plain and composite porous alumina samples boiled for different times in (a) alkali and (b) acid solutions.

Although, the percent mass loss ranges of the Al_2O_3-4Ni-10SCB composite in 10 wt% NaOH and 20 wt% H_2SO_4 (1.14-1.25 % and 1.06-1.29 %) were higher than that of the Al_2O_3-2Ni-10SCB composite (0.86-1.15 % and 1.05-1.27 %) at the early stage (2-4 h) of the corrosion test, a divergent trend to the above was observed beyond the 4h mark and in a similar sequence; the Al_2O_3-4Ni-10SCB composite exhibited percent mass losses 1.34-1.50 % and 1.59-2.16 % while 1.73-1.85 % and 2.16-2.48 % percent mass losses were registered for the Al_2O_3-2Ni-10SCB composite between 6-8h corroding time. The higher mass loss exhibited by the Al_2O_3-2Ni-10SCB composite relative to the Al_2O_3-4Ni-10SCB composite can best be explained by the lower density (Al_2O_3-2Ni-10SCB = 1.88 g/cm^3; Al_2O_3-4Ni-10SCB = 1.90 g/cm^3) observed in this particular composite. The representative FESEM micrographs of both un-corroded and corroded plain and Ni-reinforced porous alumina ceramic composites are presented in Figure 6. It can be observed that exfoliated crystal-like particles appeared on the microstructures of both the plain and composite samples. Regardless of the corrosive mediums, microstructures of the corroded composite samples exhibited more sufface fissures as compared to the plain counterpart owing to the easy dissolution of the highly vulnerable $NiAl_2O_4$ spinel phase.

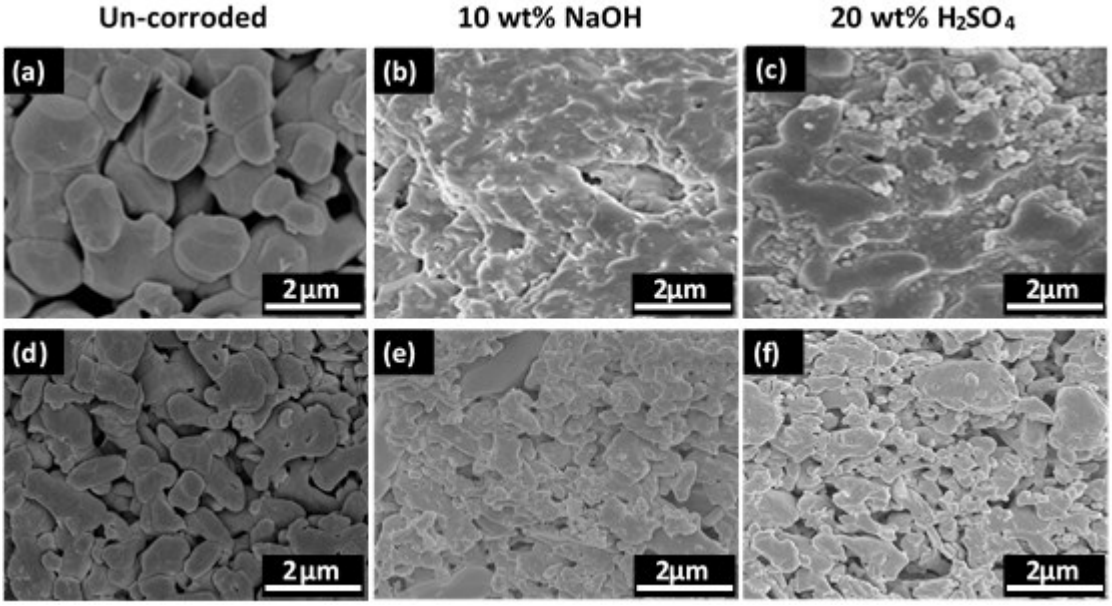

Figure 6. FESEM micrographs of (a-c) plain porous alumina ceramics and (d-e) porous alumina composite reinforced with 4 wt% Ni content.

4. Conclusion

In summary, the present work reported the fabrication of porous Al_2O_3/Ni composites with a close range of porosity (50.4-57.1 vol%) and pore size (84-109 µm) using sugarcane bagasse as the pore-forming agent. In contrast to the dominant alumina peak exhibited by the plain porous alumina, the introduction of Ni reinforcement to the alumina matrix triggered the evolution of $NiAl_2O_4$ spinel microstructure in the composite samples. Results from the corrosion resistance test showed that the samples demonstrated superior chemical stability in hot alkali solution than the acid solution. Hence, it is believed that the developed porous alumina ceramic composites are more suitable as separation membranes in alkaline mediums.

References

[1] Newnham, J., Mantri, K., Amin, M. H., Tardio, J., & Bhargava, S. K. (2012). Highly stable and active Ni-mesoporous alumina catalysts for dry reforming of methane. I*nternational journal of hydrogen energy*, *37*(2), 1454-1464.

[2] Yoon, B. H., Choi, W. Y., Kim, H. E., Kim, J. H., & Koh, Y. H. (2008). Aligned porous alumina ceramics with high compressive strengths for bone tissue engineering. *Scripta Materialia*, *58*(7), 537-540.

[3] Naik, B., Prasad, V. S., & Ghosh, N. N. (2012). Preparation of Ag nanoparticle loaded mesoporous γ-alumina catalyst and its catalytic activity for reduction of 4-nitrophenol. *Powder technology*, *232*, 1-6.

[4] Ohji, T., & Fukushima, M. (2012). Macro-porous ceramics: processing and properties. *International Materials Reviews*, *57*(2), 115-131.

[5] Qin, W., Lei, B., Peng, C., & Wu, J. (2015). Corrosion resistance of ultra-high purity porous alumina ceramic support. *Materials Letters*, *144*, 74-77.

[6] Dong, Y., Lin, B., Zhou, J. E., Zhang, X., Ling, Y., Liu, X., & Hampshire, S. (2011). Corrosion resistance characterization of porous alumina membrane supports. *Materials Characterization*, *62*(4), 409-418.

[7] Li, S., Wang, C. A., & Zhou, J. (2013). Effect of starch addition on microstructure and properties of highly porous alumina ceramics. *Ceramics International*, *39*(8), 8833-8839.
[8] Lu, J., Gao, L., Sun, J., Gui, L., & Guo, J. (2000). Effect of nickel content on the sintering behavior, mechanical and dielectric properties of Al_2O_3/Ni composites from coated powders. *Materials Science and Engineering: A*, *293*(1-2), 223-228.
[9] Chen, R. Z., & Tuan, W. H. (1999). Pressureless sintering of Al_2O_3/Ni nanocomposites. *Journal of the European Ceramic Society*, *19*(4), 463-468.
[10] Sekino, T., Nakajima, T., Ueda, S., & Niihara, K. (1997). Reduction and sintering of a nickel–dispersed-alumina composite and its properties. *Journal of the American Ceramic Society*, *80*(5), 1139-1148.
[11] Breval, E., Deng, Z., Chiou, S., & Pantano, C. G. (1992). Sol-gel prepared Ni-alumina composite materials. *Journal of materials science*, *27*(6), 1464-1468.
[12] Li, X., Yin, X., Zhang, L., Cheng, L., & Qi, Y. (2009). Mechanical and dielectric properties of porous Si_3N_4–SiO_2 composite ceramics. *Materials Science and Engineering: A*, *500*(1-2), 63-69.
[13] Sun, Y., Yang, Z., Cai, D., Li, Q., Li, H., Wang, S., & Zhou, Y. (2017). Mechanical, dielectric and thermal properties of porous boron nitride/silicon oxynitride ceramic composites prepared by pressureless sintering. *Ceramics International*, *43*(11), 8230-8235.
[14] Richter, H., & Peters, P. W. (2016). Tensile strength distribution of all-oxide ceramic matrix mini-composites with porous alumina matrix phase. *Journal of the European Ceramic Society*, *36*(13), 3185-3191.
[15] Han, D., Mei, H., Farhan, S., Xiao, S., Xia, J., & Cheng, L. (2017). Anisotropic compressive properties of porous CNT/SiC composites produced by direct matrix infiltration of CNT aerogel. *Journal of the American Ceramic Society*, *100*(5), 2243-2252.
[16] Fu, Q., Jia, W., Lau, G. Y., & Tomsia, A. P. (2018). Strength, toughness, and reliability of a porous glass/biopolymer composite scaffold. *Journal of Biomedical Materials Research Part B: Applied Biomaterials*, *106*(3), 1209-1217.
[17] Dele-Afolabi, T. T., Hanim, M. A., Norkhairunnisa, M., Sobri, S., Calin, R., & Ismarrubie, Z. N. (2018). Tensile strength and corrosion resistance properties of porous Al_2O_3/Ni composites prepared with rice husk pore-forming agent. *Ceramics International*, *44*(10), 11127-11135.
[18] Dele-Afolabi, T. T., Hanim, M. A., Norkhairunnisa, M., Sobri, S., Calin, R., & Ismarrubie, Z. N. (2018). Significant effect of rice husk and sugarcane bagasse pore formers on the microstructure and mechanical properties of porous Al_2O_3/Ni composites. *Journal of Alloys and Compounds*, *743*, 323-331.
[19] Dalconi, M. C., Cruciani, G., Alberti, A., Ciambelli, P., & Rapacciuolo, M. T. (2000). Ni2+ ion sites in hydrated and dehydrated forms of Ni-exchanged zeolite ferrierite. *Microporous and mesoporous materials*, *39*(3), 423-430.
[20] Lu, J., Gao, L., Sun, J., Gui, L., & Guo, J. (2000). Effect of nickel content on the sintering behavior, mechanical and dielectric properties of Al_2O_3/Ni composites from coated powders. *Materials Science and Engineering: A*, *293*(1-2), 223-228.
[21] Hashimoto, S., Honda, S., Hiramatsu, T., & Iwamoto, Y. (2013). Fabrication of porous spinel ($MgAl_2O_4$) from porous alumina using a template method. *Ceramics International*, *39*(2), 2077-2081.
[22] Allende-Mata, R., Almanza-Robles, J. M., Escobedo-Bocardo, J. C., & Cortés-Hernández, D. A. (2018). Corrosion of nickel aluminate by Ca, Fe, Mg and V oxides and synthetic slags. *Ceramics International, 44(14), 16522-16527*.